

Evaluation of The Selectivity, Performance, and Regeneration Capability of Ni/Cr-Gambier Leaf Extract Composites for Anionic Dyes Removal

Jefri Jefri¹, Najma Annuria Fithri², Aldes Lesbani^{1,3,*} 

¹ Master Program of Materials Science, Graduate School, Universitas Sriwijaya, Palembang, 30139, Indonesia

² Department of Pharmacy, Faculty of Mathematics and Natural Sciences, Universitas Sriwijaya, Ogan Ilir, 30862, Indonesia

³ Research Center of Inorganic Materials and Coordination Complexes, Universitas Sriwijaya, Palembang, 30139, Indonesia

* Correspondence: aldeslesbani@pps.unsri.ac.id

Scopus Author ID 15056199800

Received: 20.01.2025; Accepted: 11.04.2025; Published: 8.06.2025

Abstract: This study investigated the potential of Ni/Cr layered double hydroxide (LDH) and its composite with gambier leaf extract (GLE) as an adsorbent for anionic dye removal from the solution. Ni/Cr LDH material was synthesized via the co-precipitation method and combined with GLE to form Ni/Cr-GLE composite using aquatic solvent under nitrogen conditions. Characterization revealed significant structural changes in Ni/Cr-GLE, as seen in XRD, FT-IR, and BET analysis, which showed the integration of GLE and an increase in surface area. FT-IR analysis confirmed the presence of catechin compounds on the GLE, while BET showed a surface area of 0.65 m²/g on Ni/Cr-GLE, higher than 0.42 m²/g on Ni/Cr LDH. Selectivity studies on anionic dyes showed a high affinity of Ni/Cr-GLE towards methyl orange (MO), with a maximum adsorption capacity (Q_{max}) of 214.285 mg/g, much higher than that of 36.363 mg/g on Ni/Cr LDH. The isotherms of Ni/Cr-GLE conformed to the Freundlich model, while the adsorption kinetics followed the PSO model. In addition, the adsorption process occurs spontaneously, absorbing heat (endothermic). Regeneration results showed the ability of Ni/Cr-GLE to maintain its adsorption capacity after several reuse cycles, indicating its structural stability.

Keywords: NiCr LDH; gambier leaf extract; selectivity; methyl orange; electrostatics.

© 2025 by the authors. This article is an open-access article distributed under the terms and conditions of the Creative Commons Attribution (CC BY) license (<https://creativecommons.org/licenses/by/4.0/>), which permits unrestricted use, distribution, and reproduction in any medium, provided the original work is properly cited. The authors retain the copyright of their work, and no permission is required from the authors or the publisher to reuse or distribute this article as long as proper attribution is given to the original source.

1. Introduction

Synthetic dyes are widely used in the industrial world in both the textile and food industries [1–3]. Dyes often contain components that are difficult to decompose naturally, both cationic and anionic so that they can pollute water sources [4,5]. In addition, anionic dyes such as direct yellow, methyl orange, congo red, remazol red, and direct green are toxic and carcinogenic, which endanger ecosystems and humans [6–8]. Hence, there is a need for treatment with appropriate methods to remove these contaminants from water sources.

Among various wastewater treatment methods, adsorption is considered one of the most effective and environmentally friendly techniques for removing organic pollutants [9,10]. This method has the advantage of being relatively low-cost and easy to apply [11]. Several previous studies have proven the effectiveness of adsorption methods in the removal of anionic dye

contaminants with various types of materials such as biochar [12], bentonite [13], activated carbon [14], Layered Double hydroxide (LDH) [15].

LDH has attracted attention as an adsorbent because it has a layered structure and anions between the layers [16–18]. However, the lack of structural stability in LDH makes it difficult to reuse and less economical [19,20]. This can be overcome by modifying, such as adding support materials to LDH [21]. Support materials can be sourced from inorganic and organic materials.

Previous studies have reported improved function in LDH after modification with organic materials. Vazquez *et al.* [22] reported that the synthesis of Mg/Al LDH with tomato extract applied as an antioxidant has increased the stability of the structure so that it is not oxidized and extends its effective period. Wibiyana *et al.* [23] also reported an increased adsorption capacity of Zn/Al LDH composited with *Eucheuma cottonii* organic material, which was 384.61 mg/g and has been regenerated for 5 cycles on methyl orange adsorption. The synthesis of Zn/Al with thyme extract increased the adsorption of methylene blue to 80%, which was originally only 16% [24].

Using organic materials as support materials is an effective solution for reducing chemical waste, as it offers a more environmentally friendly alternative [25–27]. Tong *et al.* [28] reported that the adsorption of copper on gambier leaf bio-adsorbent has an adsorption capacity of 9.950 mg/g. In addition, Achmad *et al.* [29] also reported that gambier leaf bio-adsorbent was able to remove direct red 23 with a maximum capacity of 26.670 mg/g. In previous research, we have modified Ni/Fe LDH with gambier leaf extract for the adsorption of malachite green cationic dye [30]. The results showed that the structural stability of Ni/Fe gambier leaf extract was higher than that of Ni/Fe LDH, which was enhanced by the percentage of malachite green adsorption regeneration. This indicates that gambier leaves are suitable for use as LDH support material.

Gambier leaves (*Uncaria gambir*) are commonly found in Sumatera, Indonesia. Gambier leaves are widely used in herbal medicine due to their high catechin content, exceeding 90 mg of flavonoids [31,32]. Catechins have many carbonyl groups that can interact with the LDH layer [24,33], increasing the stability of the LDH structure. In addition, modifying LDH with gambier leaves can increase its surface area and adsorption capacity for absorbing contaminants such as anionic dyes.

In dye effluent treatment applications, the ability of the adsorbent material to exhibit selectivity to specific dye types is critical [34]. This selectivity ensures that the material can effectively target key pollutants in complex mixtures, such as anionic dyes often found in textile wastewater [35]. In addition, good selectivity enables higher efficiency in the adsorption process, reducing material requirements and operational costs [36]. Selectivity studies also provide deep insights into the interaction mechanisms between adsorbents and pollutants, such as electrostatic interactions, hydrogen bonding, or π - π interactions, which can be optimized for industrial-scale applications [37]. Therefore, evaluating adsorbent selectivity is crucial to ensure effectiveness under complex environmental conditions.

This study modified LDH (Ni/Cr) with gambier leaf extract (GLE) obtained by maceration technique. The composites were characterized by XRD, FT-IR, and BET surface analysis. The adsorption capacity of the composite material was tested by selectivity on 5 anionic dyes, namely direct yellow (DY), methyl orange (MO), Congo red (CR), remazol red (RR), and direct green (DG) (Figure 1). The highest adsorption percentage of the dyes was

further tested with the parameters of pH, contact time, concentration, and temperature. In addition, the stability of the structure was studied through repeated use.

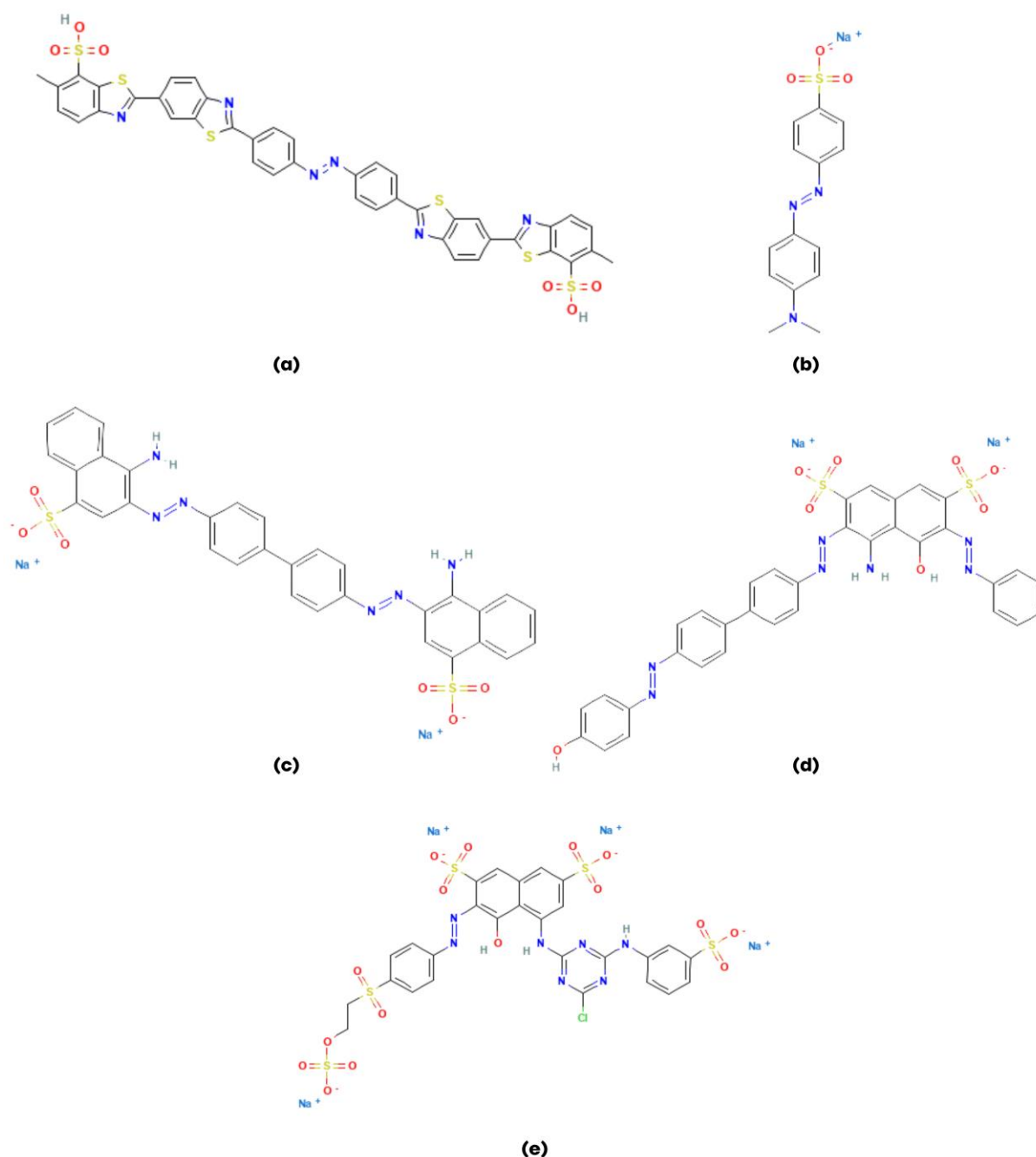


Figure 1. Structure of (a) DY; (b) MO; (c) CR; (d) RR; (e) DG [38–42]

2. Materials and Methods

2.1. Materials and instrumentals.

The materials used in this study are materials purchased without passing the purification process, including gambier (*Uncaria gambir*) leaves obtained from the South Sumatra region, anionic dyes (DY ($C_{42}H_{26}N_6O_6S$), MO ($C_{14}H_{14}N_3NaO_3S$), CR ($C_{32}H_{22}N_6Na_2O_6S_2$), RR ($C_{27}H_{18}ClN_7Na_4O_{16}S_5$), and DG ($C_{34}H_{23}N_7Na_2O_8S_2$)), nickel (II) nitrate ($Ni(NO_3)_2 \times 6H_2O$), chromium (III) nitrate ($Cr(NO_3)_3 \times 9H_2O$), sodium carbonate, sodium chloride, sodium hydroxide, ethyl acetate, hydrochloric acid (HCl) obtained from Merck, and aquadest from PT Dira Sonita Indonesia.

Furthermore, the synthesized materials were characterized with several instruments, namely Rigaku Miniflex X-Ray Diffractometer (XRD), BELSORP-miniX Brunauer-Emmett-Teller (BET) surface area analyzer, Shimadzu Prestige-21 Fourier Transform Infrared (FT-IR) spectrophotometer. The selectivity and adsorption of the materials were tested with anionic dyes measured with EMC 18 PC UV-Vis.

2.2. LDH synthesis.

Nickel (II) nitrate and chromium (III) nitrate solutions were mixed with a concentration ratio of 3:1. pH 10 was adjusted by adding 20 mL of 2 M sodium carbonate and 2 M sodium hydroxide. The mixture was precipitated by stirring (240 rpm) and heating (80°C) for 10 hours. The clay formed was filtered and baked at 105°C. The synthesized Ni/Cr LDH was crushed and characterized.

2.3. Extraction of Gambier leaves.

Gambier leaves were extracted using the maceration method. 150 mg of dried gambier leaves were soaked with 750 mL of ethyl acetate solvent for 1x24 hours. The mixture was filtered, then the extract was separated from the filtrate using a rotary evaporator at a temperature of 55°C. The gambier leaf extract (GLE) was refined and characterized by XRD and FT-IR.

2.4. Composite synthesis.

Ni/Cr LDH-GLE composite was synthesized using an aqueous solvent. LDH and GLE were mixed in 100 mL of aquadest and ultrasonicated for 45 min. Then, the mixture was reacted at 80°C for 24 hours in a nitrogen atmosphere. The formed composite was filtered and dried for further characterization.

2.5. Determination of pH point of zero charge (pHpzc).

20 mL of NaCl with a concentration of 0.1 M was varied in pH (2-11) by adding HCl and NaOH. Then, 20 mg of Ni/Cr LDH and Ni/Cr-GLE were added and shaken for 12 hours, and the final pH was measured. The initial and final pH were plotted to get the pHpzc.

2.6. Selectivity study.

Selectivity of LDH and LDH-GLE materials was carried out on several anionic dyes, namely DY, MO, RR, and DG. Each dye was made at a concentration of 20 ppm and mixed. Then, the dye mixture was scanned with UV-Vis. Furthermore, it was adsorbed with time variations of 5, 15, 30, 60, and 120 minutes with LDH and LDH-GLE materials. The remaining dye concentration was rescanned using UV-VIS, and the adsorption percentage was calculated using Equation 1 [43]. The highest capacity of anionic dyes was studied more comprehensively.

$$\% \text{ Adsorption} = \frac{(C_0 - C_t)}{C_0} \times 100\% \quad (1)$$

Where C_0 the initial concentration of dyes (mg/L) and C_t is the final concentration of dyes (mg/L).

2.7. Adsorption study.

2.7.1. Impact of pH.

20 mL of anionic dye obtained from the selectivity study was prepared at a concentration of 30 mg/L. Furthermore, the pH was varied to 5-10 by adding HCl and NaOH. Then 20 mg Ni/Cr-GLE was added and adsorbed for 2 hours. The final concentration was measured using UV-Vis, and the adsorption capacity was calculated using Equation 2. The resulting optimum pH was compared with the pH_{pzc} value. A similar experiment was conducted with Ni/Cr LDH as a control variable.

$$Q_e = \frac{(C_0 - C_t)V}{m} \quad (2)$$

Where Q_e is adsorption capacity (mg/g), m is the mass of adsorbent (g), and V is the volume of the solutions (L).

2.7.2. Impact of contact time.

Variations in contact time were studied to determine the adsorption kinetics of both materials. 20 mL of dye with a concentration of 30 mg/L and optimum pH was adsorbed with Ni/Cr LDH and Ni/Cr-GLE. Adsorption was conducted with a contact time variation of 10-120 minutes. The final concentration (C_e) was measured by UV-Vis and then used to calculate the adsorption capacity (Q_e) (Equation 2). The reaction kinetics were then determined based on the Equation of pseudo-first-order (PFO) (3) and pseudo-second-order (PSO) (4) [43].

$$\text{Log} (Q_e - Q_t) = \text{Log}Q_e - \frac{k_1}{2.303} t \quad (3)$$

$$\frac{t}{Q_t} = \frac{1}{k_2 Q_e^2} + \frac{1}{Q_e} \quad (4)$$

Where Q_t is the amount adsorbed at the time t (mg/g), k_1 is the PFO adsorption rate constant (1/min), and t is time (min). The rate constant k_1 can be determined from the slope of a linear plot of $\text{Log} (Q_e - Q_t)$ versus t . k_2 is the PSO rate constant (g/mg.min), and the rate constant k_2 can be determined from a plot of $\frac{t}{Q_t}$ versus t .

2.7.3. Impacts of concentration and temperature.

The impacts of concentration and temperature were investigated to understand the isotherms and thermodynamics involved in the adsorption process of the anionic dye. Dye concentrations were varied to 20, 30, 40, and 50 mg/L in a fixed solution volume of 20 mL. The pH of each solution was adjusted to the optimal level for adsorption. A total of 20 mg of adsorbent (Ni/Cr and Ni/Cr-GLE) was then added to each solution, and the adsorption process was conducted at optimal contact times with temperature variations set at 30, 40, 50, and 60°C. The remaining dye concentration was measured using UV-Vis spectrophotometry. The adsorption isotherms were modeled according to Langmuir and Freundlich equations (Equations 5 and 6) [44].

$$\frac{t}{Q_t} = \frac{1}{k_2 Q_e^2} + \frac{1}{Q_e} \quad (5)$$

$$\text{Log } Q_e = \text{Log } K_F + \frac{1}{n} \text{Log } C_e \quad (6)$$

In the Langmuir isotherm model, Q_{max} represents the maximum adsorption capacity while K_L is the Langmuir constant, indicating the adsorption affinity for MG. In contrast, the Freundlich isotherm describes adsorption on heterogeneous surfaces, where K_F is the Freundlich constant, reflecting adsorption strength, and n denotes the adsorption intensity.

To better understand the adsorption process, thermodynamic parameters are evaluated through experiments carried out at different temperatures. These parameters - Gibbs free energy change (ΔG°), enthalpy change (ΔH°), and entropy change (ΔS°) - help to reveal important aspects of the process, such as spontaneity, heat exchange, and changes in irregularity at the solid-liquid interface [45].

The value of ΔG° , ΔH° , and ΔS° was calculated using Equations 7 and 8.

$$\Delta G^\circ = -RT \ln K_d \quad (7)$$

$$\ln K_d = \frac{\Delta S^\circ}{R} - \frac{\Delta H^\circ}{RT} \quad (8)$$

Where K_d is the distribution coefficient, R is the gas constant, and T is the temperature in Kelvin.

2.7. Regeneration study.

Regeneration was performed to assess the structural stability of the adsorbent. A total of 20 mg of Ni/Cr and Ni/Cr-GLE adsorbents were added to 20 mL of dye solution at a concentration of 20 mg/L. The mixture was allowed to react for 2 hours, after which the final concentration was measured using UV-Vis spectrophotometry, and the adsorption capacity was calculated according to Equation 2. Following this, the adsorbent was separated from the adsorbate. The adsorbent was then immersed in 50 mL of water and desorbed through ultrasonic treatment for 30 minutes. After this treatment, the water was separated from the adsorbent, which was then dried for reuse in subsequent cycles. This regeneration process was repeated for 5 to 7 cycles.

3. Results and Discussion

3.1. Characterization of adsorbent.

The structural and functional identification of Ni/Cr LDH and Ni/Cr-GLE composite materials was conducted using XRD, FT-IR, and surface area analysis. As shown in Figure 2-a, the XRD results reveal diffraction patterns for Ni/Cr at $2\theta = 12.08^\circ$, 22.22° , 34.48° , and 61.16° , corresponding to the Miller indices (003), (006), (012), and (110), respectively (JCPDS 74-1057). These results align with previous findings reported by Chen *et al.* [46] and Gamil *et al.* [47] on Ni/Cr characterization by XRD. In the diffractogram of the Ni/Cr-GLE composite material, a shift in the (006) peak angle from 22.22° to 20.46° is observed, along with the appearance of a new peak at $2\theta = 26.12^\circ$, suggesting the incorporation of GLE. Consistent with earlier studies, a shift in the angle from 22.96° to 23.02° is also noted in the diffractogram of Ni/Fe modified with gambier leaf [48].

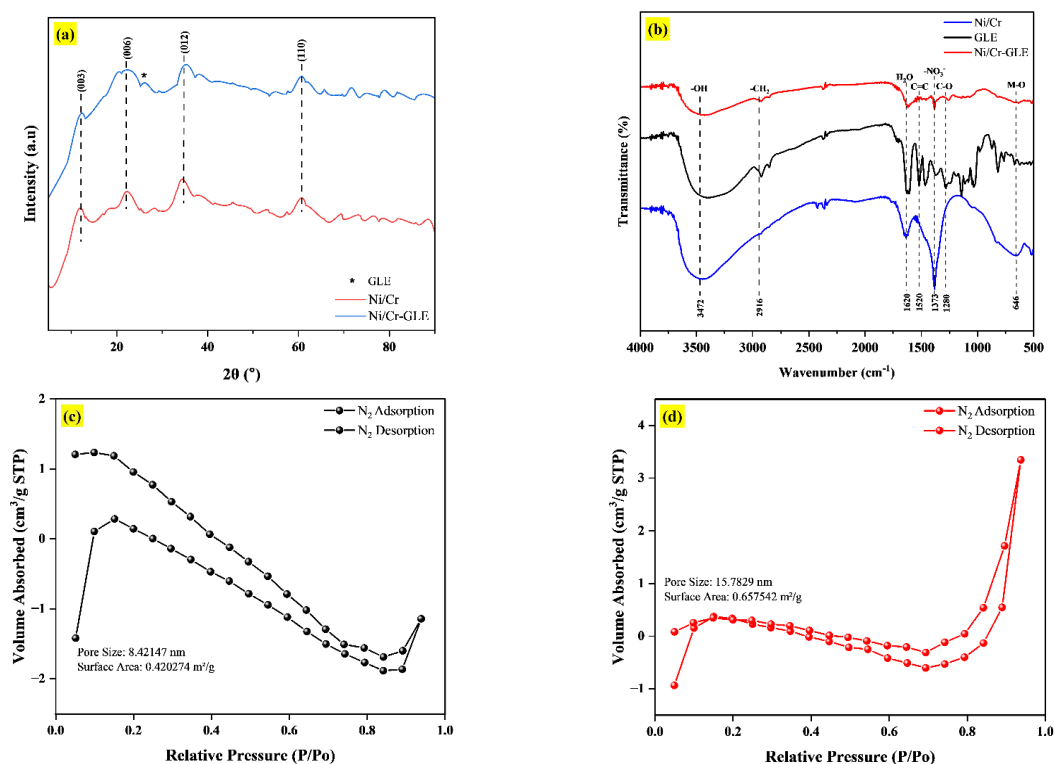


Figure 2. (a) XRD pattern; (b) FT-IR spectra; (c) N₂ adsorption-desorption of Ni/Cr LDH; (d) N₂ adsorption-desorption of Ni/Cr-GLE.

The FT-IR spectra in Figure 2-b confirm the successful incorporation of GLE, which is rich in catechins, into the Ni/Cr LDH structure. The peaks at 1280 cm⁻¹, which are associated with C-O groups, and at 1520 cm⁻¹, which indicate aromatic C=C bonds [49], support the presence of catechin compounds in the Ni/Cr-GLE composite. In addition, the peak at 1387 cm⁻¹, which indicates the presence of NO₃⁻ anion in the interlayer [50], indicates that the LDH structure retains its interlayer interaction despite the modification.

The peak at 2916 cm⁻¹ is related to -CH₂ vibrations, indicating the presence of aliphatic groups of organic compounds in gambier extract. On the other hand, the peak at 646 cm⁻¹ is derived from M-O vibrations [51], indicating the metal-oxygen bonds in the LDH structure are preserved. The peak at 1620 cm⁻¹ is related to the deformation of water molecules [52], indicating the presence of absorbed water in the LDH layer structure. The presence of these organic groups strengthens the adsorption ability of the composite material, which is also supported by the changes in crystal structure observed in the XRD results.

BET images 2-c and 2-d show the nitrogen adsorption/desorption isotherms for Ni/Cr LDH and Ni/Cr-GLE, which belong to type IV with hysteresis type H3. Type IV isotherms are characteristic of mesoporous materials, which is corroborated by the average pore size of 8.42 nm for Ni/Cr LDH and 15.78 nm for Ni/Cr-GLE. Type H3 hysteresis is usually associated with layered particles or slit-like pores [53], indicating that the pore structure in these two materials supports the adsorption capacity.

On Ni/Cr LDH (Figure 2-c), the relatively small surface area of 0.42 m²/g indicates a limited active area for adsorbate molecule interaction. However, after adding GLE to Ni/Cr-GLE (Figure 2-d), the surface area increased to 0.65 m²/g, and the pore size became larger. This increase indicates that the gambier extract provides structural modification, which expands the surface area and pores, thereby increasing the adsorption capacity.

3.2. Selectivity of anionic dyes.

Selectivity tests were conducted to evaluate the adsorbent's ability to adsorb various types of anionic dyes, such as DY, MO, CR, RR, and DG. Using Ni/Cr LDH and Ni/Cr-GLE materials, this selectivity analysis aims to understand dyes' effectiveness and adsorption tendency with different chemical structures. This test is very important for practical applications, especially in wastewater treatment, where various dyes require the adsorbent material to have a good selective ability to adsorb various contaminants with high efficiency.

The results in Figure 3-a,b show that Ni/Cr LDH and Ni/Cr-GLE can decrease the dye's absorbance over time, with Ni/Cr-GLE showing a more significant decrease. However, since the absorbance curves for each time tend to overlap, deconvolution is required to separate and identify the overlapping spectral components, as shown in Figure 3-c,d. This deconvolution helps interpret the adsorption results more clearly, enabling a more detailed analysis of each dye's kinetics and adsorption mechanisms.

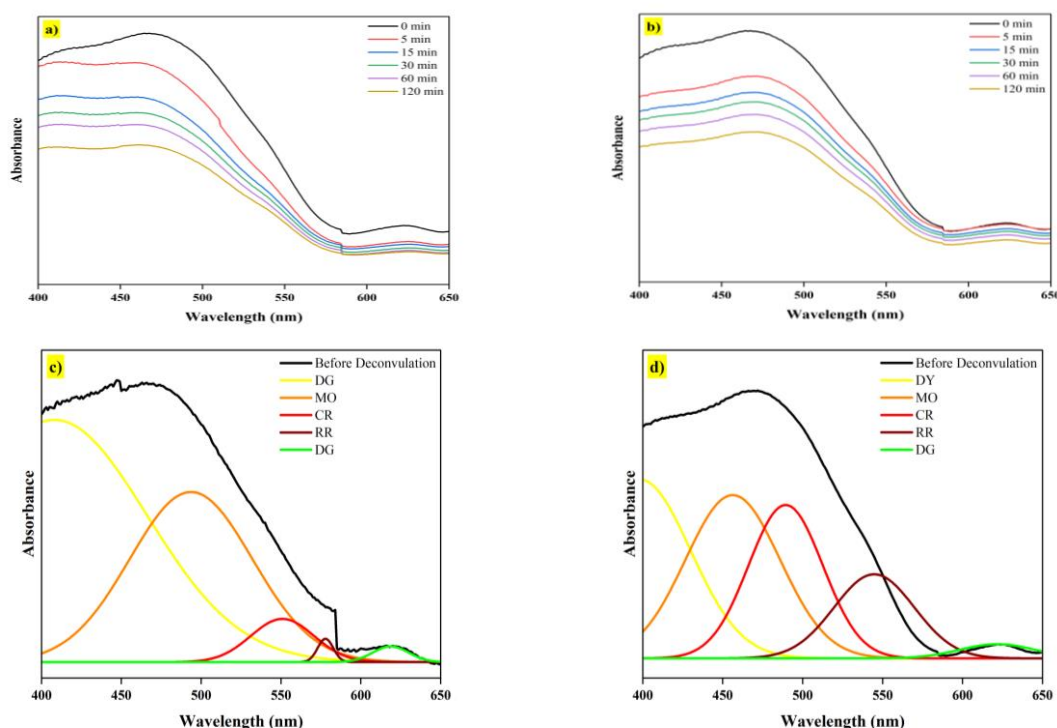


Figure 3. Selectivity of anionic dyes' absorbance (0-120 minutes) by (a) Ni/Cr LDH; (b) Ni/Cr-GLE, and deconvolution of anionic dyes' absorbance using Gaussian curve fit of (c) Ni/Cr LDH; (d) Ni/Cr-GLE.

Based on the adsorption percentage data (Table 1), it can be seen that Ni/Cr LDH and Ni/Cr-GLE materials show different selectivity towards various anionic dyes, with both having the highest adsorption for MO. This suggests that Ni/Cr and Ni/Cr-GLE materials have a high affinity for MO compared to other anionic dyes such as DY, CR, RR, and DG. The interaction between the functional groups on MO and the material surface plays an important role in this selectivity.

The high selectivity towards MO can be explained by the strong electrostatic interaction between MO anions and the surface of Ni/Cr LDH and Ni/Cr-GLE materials. These materials contain a hydroxide layer with a positive charge that can attract MO anions through electrostatic attraction [54]. In addition, the aromatic structure and specific functional groups on MO may more suitably interact with the active sites on the surface of these materials [30], thereby enhancing adsorption. This selectivity is important in sewage treatment applications as

it shows that Ni/Cr LDH and Ni/Cr-GLE are more effective in targeting and removing MO than other anionic dyes.

Table 1. Percentages of anionic dye adsorption.

Dyes	% Adsorption	
	Ni/Cr	Ni/Cr-GLE
DY	64.486	44.886
MO	67.371	47.332
CR	66.817	32.220
RR	63.896	31.582
DG	4.155	26.650

3.3. Adsorption study.

In this study, the analysis of pH_{pzc} of materials, optimum pH, adsorption kinetics, adsorption isotherms, and thermodynamics provides an in-depth understanding of the effectiveness of Ni/Cr LDH and Ni/Cr-GLE in adsorbing MO. Based on Figure 4-a, the pH_{pzc} values for Ni/Cr LDH and Ni/Cr-GLE are 7.00 and 7.23, respectively, indicating that the material surface will be positively charged at pH below this value and negatively charged at pH above it. This condition is important because MO is an anionic dye that will be more attracted to positively charged surfaces. Hence, pH values below pH_{pzc} favor strong electrostatic interactions with MO anions [35].

Figure 4-b shows that the optimum pH for MO adsorption is 5, below pH_{pzc}. At this pH, Ni/Cr LDH and Ni/Cr-GLE surfaces are sufficiently positively charged, thus supporting the electrostatic attraction towards MO anions and increasing the adsorption capacity [55]. This interaction maximizes the adsorption efficiency by directing MO to active sites on the adsorbent surface, accelerating the achievement of adsorption equilibrium.

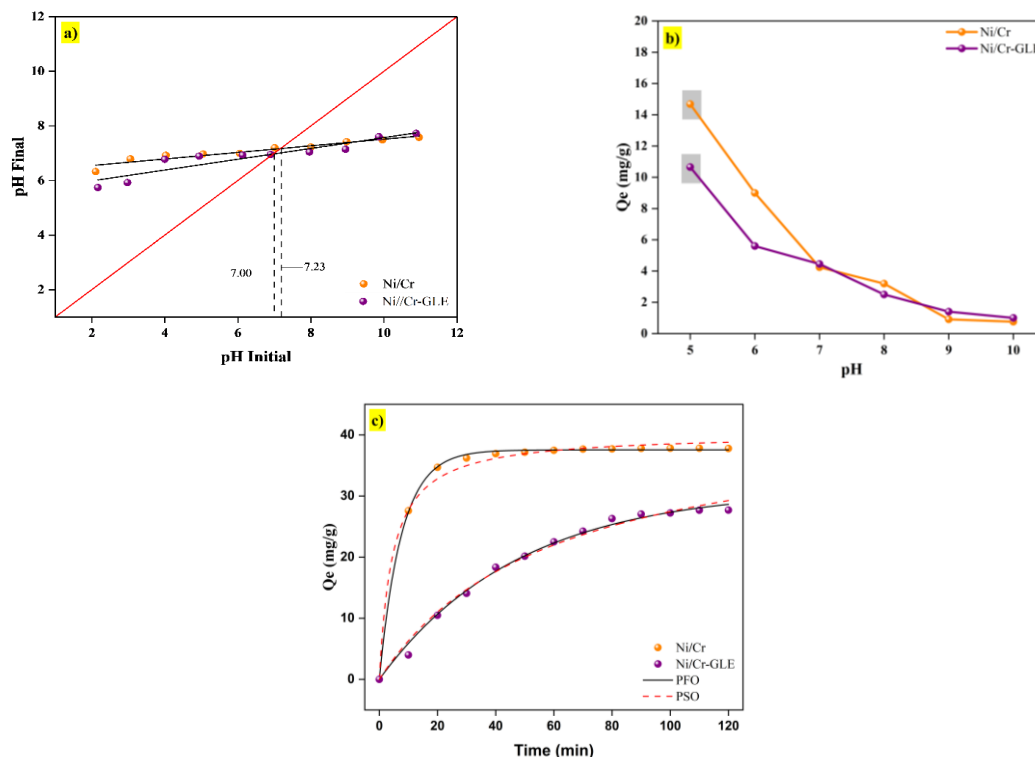


Figure 4. (a) pH_{pzc}; (b) pH optimum; (c) Kinetics of Ni/Cr LDH and Ni/Cr-GLE.

The adsorption study revealed that the optimal contact times for effective dye removal were 70 minutes for Ni/Cr LDH and 80 minutes for Ni/Cr-GLE. Furthermore, Figure 4-c

illustrates the adsorption kinetics, showing that Ni/Cr-GLE fits the Pseudo-Second Order (PSO) model better, while Ni/Cr LDH fits the Pseudo-First Order (PFO) model better. This can be seen from the higher R^2 values of each model, 0.998 for PSO on Ni/Cr-GLE and 0.999 for PFO on Ni/Cr LDH, indicating a good fit between the model and the experimental data (see Table 2).

Table 2. The kinetics parameter of PFO and PSO of Ni/Cr LDH and Ni/Cr-GLE.

Materials	PFO				PSO		
	$Q_{e,exp}$	$Q_{e,calc}$	K_1	R^2	$Q_{e,calc}$	k_2	R^2
NiCr	37.671	37.545	0.131	0.999	40.264	0.005	0.958
NiCr-GLE	37.692	31.161	0.021	0.993	43.702	3.862	0.998

On Ni/Cr-GLE, the PSO model produced a $Q_{e,calc}$ value of 43.702 mg/g, close to Q_{exp} of 37.692 mg/g. This indicates that the adsorption kinetics of Ni/Cr-GLE follow the PSO mechanism, indicating significant chemical interactions between MO and the active sites formed by the functional groups of GLE on the material surface [30].

In contrast, the adsorption on Ni/Cr LDH is more in line with the PFO model, with 37.545 mg/g, which is close to $Q_{e,calc}$'s 37.671 mg/g. This suggests that the adsorption process on Ni/Cr LDH is controlled by a more dominant physical mechanism, with the adsorption rate being more dependent on the initial interaction between the MO and the material surface.

This difference in adsorption mechanism highlights the effect of surface modification by GLE on Ni/Cr-GLE, strengthening the chemical interactions and thus better fits the PSO model. This indicates that Ni/Cr-GLE has more potential for applications that require strong chemical adsorption, while Ni/Cr LDH is more suitable for applications influenced by physical interactions.

Based on the data from Table 3, the adsorption isotherms of MO on Ni/Cr LDH and Ni/Cr-GLE showed different results at various temperatures, indicating the great influence of material modification with GLE on the maximum adsorption capacity (Q_{max}). Ni/Cr-GLE had a higher Q_{max} at 60°C, which amounted to 214.29 mg/g, compared to Ni/Cr LDH, which only reached 36.36 mg/g at the same temperature. This significant increase is thought to be due to the presence of active functional groups on GLE, such as hydroxyl (-OH) and carbonyl (C=O) groups, which can interact strongly with MO molecules through hydrogen bonding and electrostatic interactions [56], thus increasing the number of active sites on the adsorbent surface. In addition, BET characteristics show that Ni/Cr-GLE has a better mesoporous structure, enabling more efficient diffusion of MO molecules into the pores and favoring an increased adsorption capacity.

Table 3. The adsorption isotherm Langmuir and Freundlich Ni/Cr LDH and Ni/Cr-GLE.

Material	T (°C)	Langmuir			Freundlich		
		Q_{max}	k_L	R^2	n	k_F	R^2
Ni/Cr LDH	30	14.556	0.014	0.126	0.671	0.954	0.492
	40	76.923	0.007	0.009	0.821	2.011	0.840
	50	28.653	0.018	0.353	1.316	5.269	0.526
	60	36.363	0.223	0.526	2.532	1.002	0.888
Ni/Cr-GLE	30	39.840	0.006	0.042	0.870	1.488	0.653
	40	40.816	0.015	0.038	2.533	1.002	0.330
	50	80.000	0.012	0.101	1.316	5.269	0.760
	60	214.285	0.001	0.005	1.012	47.393	0.936

The Freundlich isotherm model better fits both materials at several temperatures, with higher R^2 values than the Langmuir model. This indicates that adsorption occurs on a heterogeneous surface [57], where the parameter n greater than 1 indicates that the adsorption intensity increases as the MO concentration increases. Especially for Ni/Cr-GLE, the strong interaction between the functional groups of GLE and MO molecules further strengthens the adsorption capacity, making this material more effective in adsorbing MO than Ni/Cr LDH. A comparison of these Q_{max} values with those reported in previous studies on methyl orange adsorption is provided in Table 4, further demonstrating the enhancement achieved with GLE modification.

Table 4. The comparison of Q_{max} of methyl orange adsorption.

Materials	Q_{max} (mg/g)	References
Chitosan bead-like	12.460	[58]
<i>Stipa tenacissima</i> L	16.940	[59]
Zn/Co/Fe LDH-chitosan	165.890	[60]
Mg/Al LDH	197.620	[61]
Corn cob biochar	86.380	[62]
Chrysotile nanotubes	31.460	[63]
Bentonite	308.000	[13]
Activated carbon	42.600	[64]
Ni/Cr LDH	36.363	This Study
Ni/Cr-GLE	214.285	This Study

The thermodynamic parameters obtained for the adsorption process with Ni/Cr and Ni/Cr-GLE showed some important characteristics. The positive enthalpy change (ΔH°) values, 35.176 kJ/mol for Ni/Cr and 27.824 kJ/mol for Ni/Cr-GLE (see Table 5) indicate that the adsorption process is endothermic [65]. The higher ΔH° value for Ni/Cr indicates that this material requires more energy to adsorb the dye compared to Ni/Cr-GLE. This difference may be due to the presence of catechin functional groups from GLE on Ni/Cr-GLE, which allows the adsorption process to occur more efficiently with lower energy requirements.

Table 5. Thermodynamic parameters of Ni/Cr and Ni/Cr-GLE.

Materials	Conc. (mg/L)	ΔH° (kJ/mol)	ΔS° (J/mol.K)	ΔG° (kJ/mol)			
				303 K	313 K	323 K	333 K
Ni/Cr	50	35.176	0.108	1.567	0.152	-1.263	-2.678
Ni/Cr-GLE	50	27.824	0.084	2.038	1.305	0.5718	-0.161

In addition, the positive entropy change (ΔS°), 0.108 kJ/mol-K for Ni/Cr and 0.084 kJ/mol-K for Ni/Cr-GLE indicates an increase in disorder at the solid-liquid interface during the adsorption process [66]. The higher ΔS° for Ni/Cr indicates that its adsorption produces more disorder in the system, possibly due to less organized interactions than Ni/Cr-GLE. The slight decrease in entropy values for Ni/Cr-GLE may be due to stronger and more structured interactions facilitated by the functional groups of the GLE [30].

The change in Gibbs free energy (ΔG°) values varied as the temperature increased, reflecting the spontaneity of the adsorption process [67]. At low temperatures (303 K and 313 K), both materials show positive ΔG° values, indicating that the adsorption is not spontaneous [60]. However, as the temperature rises to 323 K and 333 K, ΔG becomes negative, indicating that the adsorption process becomes spontaneous at higher temperatures [68]. In the Ni/Cr material, the ΔG value transitions from positive to negative between 313 K and 323 K, which means that the adsorption becomes more favorable above the ambient temperature of 313 K. At 333 K, ΔG° is more negative (-2.6787 kJ/mol), indicating that the adsorption becomes more

spontaneous as the temperature increases. Meanwhile, Ni/Cr-GLE also shows a transition towards negative ΔG° at 333 K, although the ΔG° value is close to zero, indicating that this material is less spontaneous than Ni/Cr at high temperatures. This may be due to the specific interactions of the Ni/Cr-GLE material that limit spontaneous adsorption.

Thus, this analysis shows that Ni/Cr-GLE with gambier extract modification offers a slightly more energy-efficient adsorption process and has more structured interactions. However, its spontaneity is lower than that of Ni/Cr, indicating that Ni/Cr-GLE may be more suitable for controlled adsorption applications or in systems where temperature regulation is possible. 3.4. Regeneration of materials.

The regeneration results in Figure 5 show that although the initial adsorption capacity of Ni/Cr is higher, at 69.17%, compared to Ni/Cr-GLE, the stability of Ni/Cr-GLE is far superior at each regeneration cycle. Ni/Cr experienced a drastic decrease of more than 20% in the second cycle, dropping from 69.17% to 40%, and continued to decrease until it reached 23.7% in the seventh cycle. In contrast, Ni/Cr-GLE maintained a more stable adsorption capacity, despite the decrease, but more moderate in each cycle, from 52.77% at the beginning of regeneration to 44.43% in the seventh cycle. The stability of Ni/Cr-GLE is thought to be due to the presence of additional functional groups from GLE on the adsorbent surface, which strengthens the material's adsorption capacity and structural resistance during the regeneration process. Thus, as seen in Figure 5, Ni/Cr-GLE has the advantage of stability for repeated use in sewage treatment applications, making it a more efficient choice than unmodified Ni/Cr.

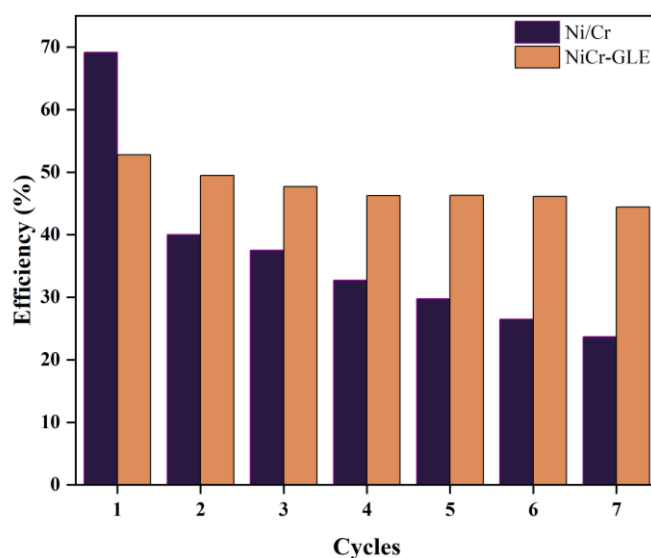


Figure 5. Regeneration of Ni/Cr LDH and Ni/Cr-GLE in seven cycles.

3.5. Mechanism of adsorption.

The FT-IR analysis in Figure 6-a provides evidence supporting the adsorption mechanism illustrated in Figure 6-b. The rise in the O–H stretching band at 3746 cm^{-1} indicates enhanced hydrogen bonding interactions between hydroxyl groups on Ni/Cr-GLE and MO molecules [69]. The increased intensity of the -NO_3^- peak at 1380 cm^{-1} suggests a stronger interaction or stabilization of nitrate ions due to electrostatic effects after MO adsorption [70]. Similarly, the heightened C–O peak at 1273 cm^{-1} and M–O vibrations at 646 cm^{-1} reflect stronger interactions between MO molecules and functional groups or metal sites on the composite. These consistent intensity increases validate the proposed adsorption mechanism,

where GLE modification introduces functional groups that amplify hydrogen bonding and electrostatic forces, enhancing the adsorption efficiency of Ni/Cr-GLE for MO.

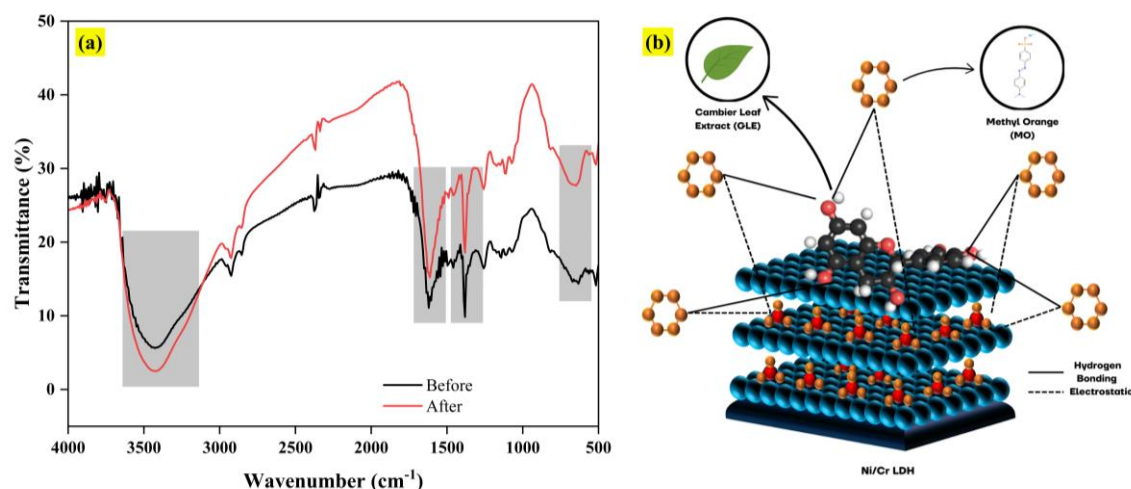


Figure 6. (a) Spectra FTIR after adsorption; (b) mechanism of adsorption MO by Ni/Cr-GLE.

4. Conclusions

The characterization of Ni/Cr LDH and Ni/Cr-GLE adsorbents showed significant structural and functional changes after adding GLE, which was confirmed through XRD, FT-IR, and BET analysis results. XRD results showed a shift and appearance of new peaks, indicating the integration of GLE into the LDH structure. FT-IR spectra confirmed the presence of catechin compounds from GLE, such as C-O groups, aromatic C=C, and -CH₂ groups, which supported the increased adsorption capacity. BET analysis showed an increase in surface area from 0.42 m²/g in Ni/Cr LDH to 0.65 m²/g in Ni/Cr-GLE, as well as a mesoporous structure with H3-type hysteresis suitable for high adsorption capacity. Selectivity test results revealed that Ni/Cr LDH and Ni/Cr-GLE have a stronger affinity to the MO. The maximum adsorption capacity (Q_{max}) value drastically increased, from 36.363 mg/g in Ni/Cr LDH to 214.285 mg/g in Ni/Cr-GLE, reflecting the enhanced effectiveness after modification. This adsorption study followed the Freundlich isotherm model and the PSO kinetics model, indicating that chemical interactions were dominant on Ni/Cr-GLE compared to the physical mechanism that dominated on Ni/Cr LDH.

Author Contributions

Conceptualization, J.J., N.A.F., and A.L.; methodology, N.A.F. and A.L.; software, J.J.; validation, N.A.F.; formal analysis, —; investigation, J.J.; resources, —; data curation, —; writing—original draft preparation, J.J.; writing—review and editing, A.L.; visualization, N.A.F.; supervision, A.L.; project administration, —; funding acquisition, —. All authors have read and agreed to the published version of the manuscript.

Institutional Review Board Statement

Not applicable.

Informed Consent Statement

Not applicable.

Data Availability Statement

Data supporting the findings of this study are available upon reasonable request from the corresponding author.

Funding

This research received no external funding.

Acknowledgments

We extend our sincere gratitude to the Research Center of Inorganic Materials and Complexes, Faculty of Mathematics and Natural Sciences, Universitas Sriwijaya, for their invaluable support and assistance in completing this research.

Conflicts of Interest

The authors declare no conflict of interest.

References

1. Slama, H. Ben; Bouket, A.C.; Pourhassan, Z.; Alenezi, F.N.; Silini, A.; Cherif-Silini, H.; Oszako, T.; Luptakova, L.; Golińska, P.; Belbahri, L. Diversity of Synthetic Dyes from Textile Industries, Discharge Impacts and Treatment Methods. *Applied Sciences (Switzerland)* **2021**, *11*, doi:10.3390/app11146255.
2. Sharma, J.; Sharma, S.; Soni, V. Classification and Impact of Synthetic Textile Dyes on Aquatic Flora: A Review. *Reg Stud Mar Sci* **2021**, *45*, 101802, doi:<https://doi.org/10.1016/j.rsma.2021.101802>.
3. Alegbe, E.O.; Uthman, T.O. A Review of History, Properties, Classification, Applications and Challenges of Natural and Synthetic Dyes. *Heliyon* **2024**, *10*, doi:10.1016/j.heliyon.2024.e33646.
4. Alsukaibi, A.K.D. Various Approaches for the Detoxification of Toxic Dyes in Wastewater. *Processes* **2022**, *10*, doi:10.3390/pr10101968.
5. Periyasamy, A.P. Recent Advances in the Remediation of Textile-Dye-Containing Wastewater: Prioritizing Human Health and Sustainable Wastewater Treatment. *Sustainability (Switzerland)* **2024**, *16*, doi:10.3390/su16020495.
6. Siddiqui, S.I.; Allehyani, E.S.; Al-Harbi, S.A.; Hasan, Z.; Abomuti, M.A.; Rajor, H.K.; Oh, S. Investigation of Congo Red Toxicity towards Different Living Organisms: A Review. *Processes* **2023**, *11*, doi:10.3390/pr11030807.
7. Valli Nachiyar, C.; Rakshi, A.D.; Sandhya, S.; Britlin Deva Jebasta, N.; Nellore, J. Developments in Treatment Technologies of Dye-Containing Effluent: A Review. *Case Studies in Chemical and Environmental Engineering* **2023**, *7*, 100339, doi:<https://doi.org/10.1016/j.cscee.2023.100339>.
8. Ibrahim, A.; El-Fakharany, E.M.; Abu-Serie, M.M.; Elkady, M.F.; Eltarahony, M. Methyl Orange Biodegradation by Immobilized Consortium Microspheres: Experimental Design Approach, Toxicity Study and Bioaugmentation Potential. *Biology (Basel)* **2022**, *11*, doi:10.3390/biology11010076.
9. Srivatsav, P.; Bhargav, B.S.; Shanmugasundaram, V.; Arun, J.; Gopinath, K.P.; Bhatnagar, A. Biochar as an Eco-Friendly and Economical Adsorbent for the Removal of CColorants (Dyes) from Aqueous Environment: A Review. *Water (Switzerland)* **2020**, *12*.

10. Quang, H.H.P.; Dinh, N.T.; Truong, Q.-M.; Nguyen, P.K.T.; Nguyen, V.-H. Unlocking the Potential of Environmentally Friendly Adsorbent Derived from Industrial Wastes: A Review. *Chemosphere* **2024**, *367*, 143662, doi:<https://doi.org/10.1016/j.chemosphere.2024.143662>.
11. Jani, Y. Adsorption: A Cost-Effective Wastewater Treatment Technology for Removal of Conventional and Emerging Organic Contaminants. In *Cost Efficient Wastewater Treatment Technologies*; Springer, 2022; p. 17 ISBN 978-3-031-12901-8.
12. Ramath, R.; Sukumaran, A.M.; Ramachandran, A.; Basheer, S.B. Methyl Orange Dye Adsorption and Degradation at Low Temperature Using Iron Oxide-Incorporated Biochar Derived from Industrial by-Products. *Bioresour Technol Rep* **2023**, *22*, 101470, doi:[10.1016/J.BITEB.2023.101470](https://doi.org/10.1016/J.BITEB.2023.101470).
13. Bessaha, F.; Bessaha, G.; Ziane, S.; Khelifa, A. Adsorption of Methyl Orange on Bentonite: Design, Modeling, and Analysis of Experiments. *Iranian Journal of Chemistry and Chemical Engineering* **2023**, *42*, 3306–3323, doi:[10.30492/ijcce.2023.1971110.5663](https://doi.org/10.30492/ijcce.2023.1971110.5663).
14. Serban, G.V.; Iancu, V.I.; Dinu, C.; Tenea, A.; Vasilache, N.; Cristea, I.; Niculescu, M.; Ionescu, I.; Chiriac, F.L. Removal Efficiency and Adsorption Kinetics of Methyl Orange from Wastewater by Commercial Activated Carbon. *Sustainability (Switzerland)* **2023**, *15*, 12939, doi:[10.3390/su151712939](https://doi.org/10.3390/su151712939).
15. Cao, Y.; Zhang, J.; Li, J.; Zhou, P.; Liu, B. Template-Free Synthesis of ZnNiAl-LDH and LDO Microspheres for Adsorption of Methyl Orange. *Russian Journal of Physical Chemistry A* **2022**, *96*, 2992–2999, doi:[10.1134/S0036024422130234](https://doi.org/10.1134/S0036024422130234).
16. Qian, J.; Zhang, Y.; Chen, Z.; Du, Y.; Ni, B.J. NiCo Layered Double Hydroxides/NiFe Layered Double Hydroxides Composite (NiCo-LDH/NiFe-LDH) Towards Efficient Oxygen Evolution in Different Water Matrices. *Chemosphere* **2023**, *345*, 140472, doi:[10.1016/J.CHEMOSPHERE.2023.140472](https://doi.org/10.1016/J.CHEMOSPHERE.2023.140472).
17. Mostafa, M.S.; Lan, C.; Selim, M.S.; Ruiyi, Z.; Ya, G.; Shuai, Z.; Ge, G. Synthesis of Novel CoBiTi LDH and Fabrication of LDH-LDO 3D-Heterojunction for Enhanced Infrared Induced Water Splitting to Hydrogen. *J Clean Prod* **2022**, *340*, 130663, doi:[10.1016/J.JCLEPRO.2022.130663](https://doi.org/10.1016/J.JCLEPRO.2022.130663).
18. Liu, Y.; Yu, Z.; Wang, Q.; Zhu, X.; Long, R.; Li, X. Application of Sodium Dodecyl Sulfate Intercalated CoAl LDH Composite Materials (RGO/PDA/SDS-LDH) in Membrane Separation. *Appl Clay Sci* **2021**, *209*, 106138, doi:[10.1016/J.CLAY.2021.106138](https://doi.org/10.1016/J.CLAY.2021.106138).
19. Rohmatullaili; Ahmad, N.; Erviana, D.; Zultriana; Savira, D.; Mohadi, R.; Lesbani, A. High Stability and Selectivity of Butterfly Pea Flower Extract-NiAl LDH-Based Catalysts in the Tetracycline Degradation. *Environmental Science and Pollution Research* **2024**, *31*, 33107–33119, doi:[10.1007/s11356-024-33445-0](https://doi.org/10.1007/s11356-024-33445-0).
20. Yuliasari, N.; Badri, A.F.; Wijaya, A.; Siregar, P.M.S.B.N.; Amri; Mardiyanto; Mohadi, R.; Lesbani, A. Modification of Mg/Al-LDH Intercalated Metal Oxide (Mg/Al-Ni) to Improve The Performance of Methyl Orange and Methyl Red Dyes Adsorption Process. *Science and Technology Indonesia* **2022**, *7*, 275–283, doi:[10.26554/sti.2022.7.3.275-283](https://doi.org/10.26554/sti.2022.7.3.275-283).
21. Wibiyani, S.; Royani, I.; Lesbani, A. Synthesis and Performance of ZnAl@Layered Double Hydroxide Composites with *Eucheuma Cottonii* for Adsorption and Regeneration of Congo Red Dye. *Indonesian Journal of Environmental Management and Sustainability* **2024**, *8*, 126–134, doi:[10.26554/ijems.2024.8.3.126-134](https://doi.org/10.26554/ijems.2024.8.3.126-134).
22. Vazquez, R.N.M.; Nuñez, C.P.; Kovalenko, V.; Kotok, V.; Moisés, F.P.P.; Lamas, A.M.M.; Arizaga, G.G.C. Electron Transfer within an Antioxidant Powder Composite with Layered Double Hydroxide Nanoparticles and Tomato Extract. *Biointerface Res Appl Chem* **2023**, *13*, doi:[10.33263/BRIAC133.257](https://doi.org/10.33263/BRIAC133.257).
23. Wibiyani, S.; Royani, I.; Ahmad, N.; Lesbani, A. Assessing the Efficiency, Selectivity, and Reusability of ZnAl-Layered Double Hydroxide and *Eucheuma Cottonii* Composite in

- Removing Anionic Dyes from Wastewater. *Inorg Chem Commun* **2024**, *170*, 113347, doi:<https://doi.org/10.1016/j.inoche.2024.113347>.
24. Bagherzadeh, M.; Salehi, G.; Rabiee, N. Rapid and Efficient Removal of Methylene Blue Dye from Aqueous Solutions Using Extract-Modified Zn–Al LDH. *Chemosphere* **2024**, *350*, 141011, doi:<https://doi.org/10.1016/j.chemosphere.2023.141011>.
 25. Abera, Y.A. Sustainable Building Materials: A Comprehensive Study on Eco-Friendly Alternatives for Construction. *Composites and Advanced Materials* **2024**, *33*, 26349833241255956, doi:10.1177/26349833241255957.
 26. Mishra, K.; Siwal, S.S.; Nayaka, S.C.; Guan, Z.; Thakur, V.K. Waste-to-Chemicals: Green Solutions for Bioeconomy Markets. *Science of The Total Environment* **2023**, *887*, 164006, doi:<https://doi.org/10.1016/j.scitotenv.2023.164006>.
 27. Kameliya, J.; Verma, A.; Dutta, P.; Arora, C.; Vyas, S.; Varma, R.S. Layered Double Hydroxide Materials: A Review on Their Preparation, Characterization, and Applications. *Inorganics (Basel)* **2023**, *11*, doi:10.3390/inorganics11030121.
 28. Tong, K.S.; Kassim, M.J.; Azraa, A. Adsorption of Copper Ion from Its Aqueous Solution by a Novel Biosorbent *Uncaria Gambir*: Equilibrium, Kinetics, and Thermodynamic Studies. *Chemical Engineering Journal* **2011**, *170*, 145–153, doi:<https://doi.org/10.1016/j.cej.2011.03.044>.
 29. Achmad, A.; Kassim, J.; Kim Suan, T.; Che Amat, R.; Lean See, T. Equilibrium, Kinetic and Thermodynamic Studies on the Adsorption of Direct Dye onto a Novel Green Adsorbent Developed from *Uncaria Gambir* Extract. *Journal of Physical Science* **2012**, *23*, 1–13.
 30. Jefri, J.; Fithri, N.A.; Lesbani, A. Enhanced Removal Efficiency of Malachite Green Dye Using *Gambir* Leaf Extract-Modified NiFe LDH Composites: A Study of Cationic Dye Adsorption. *Bulletin of Chemical Reaction Engineering & Catalysis* **2024**, *19*, 573–584, doi:10.9767/bcrec.20215.
 31. Pramanik, F.; Satari, M.H.; Azhari, A. Cytotoxic Activity of Gambier Leave (*Uncaria Gambir*) Ethyl Acetate Extract on Mouse Embryonic Fibroblast Cell (NIH-3T3) Using MTT Assay. *Open Dent J* **2023**, *17*, doi:10.2174/18742106-v17-e230109-2022-78.
 32. Noordin Kassim, J.; Hazwan Hussin, M.; Hazwani Dahon, N. Determination of Total Phenol, Condensed Tannin and Flavonoid Contents and Antioxidant Activity of *Uncaria Gambir* Extracts. *Majalah Farmasi Indonesia* **2011**, *22*, 50–59, doi:10.14499/INDONESIANJPHARMOISSOPP50-59.
 33. Kim, H.J.; Lee, G.J.; Choi, A.J.; Kim, T.H.; Kim, T. II; Oh, J.M. Layered Double Hydroxide Nanomaterials Encapsulating *Angelica Gigas* Nakai Extract for Potential Anticancer Nanomedicine. *Front Pharmacol* **2018**, *9*, doi:10.3389/fphar.2018.00723.
 34. Lv, G.; Liu, J.; Xiong, Z.; Zhang, Z.; Guan, Z. Selectivity Adsorptive Mechanism of Different Nitrophenols on UiO-66 and UiO-66-NH₂ in Aqueous Solution. *J Chem Eng Data* **2016**, *61*, 3868–3876, doi:10.1021/acs.jced.6b00581.
 35. Putra Hidayat, A.R.; Zulfa, L.L.; Widyanto, A.R.; Abdullah, R.; Kusumawati, Y.; Ediati, R. Selective Adsorption of Anionic and Cationic Dyes on Mesoporous UiO-66 Synthesized Using a Template-Free Sonochemistry Method: Kinetic, Isotherm and Thermodynamic Studies. *RSC Adv* **2023**, *13*, 12320–12343, doi:10.1039/d2ra06947d.
 36. O. Ighalo, J.; Omoarukhe, F.; Victor, O.; Iwuozor, K.; Igwegbe, C. Cost of Adsorbent Preparation and Usage in Wastewater Treatment: A Review. *Cleaner Chemical Engineering* **2022**, *3*, doi:10.1016/j.clce.2022.100042.
 37. Wu, Z.; Ye, X.; Liu, H.; Zhang, H.; Liu, Z.; Guo, M.; Li, Q.; Li, J. Interactions between Adsorbents and Adsorbates in Aqueous Solutions. *Pure and Applied Chemistry* **2020**, *1*, doi:10.1515/pac-2019-1110.
 38. National Center for Biotechnology Information PubChem Compound Summary for CID 433256, Direct Yellow 29 2024.

39. National Center for Biotechnology Information PubChem Compound Summary for CID 23673835, Methyl Orange 2024.
40. National Center for Biotechnology Information PubChem Compound Summary for CID 11313, Congo Red 2024.
41. National Center for Biotechnology Information PubChem Compound Summary for CID 166507, Reactive Red 198 2024.
42. National Center for Biotechnology Information PubChem Compound Summary for CID 135506439, C.I. Direct Green 1 2024.
43. Lalikoglu, M. Mg-Al Layered Double Hydroxide (LDH) as an Adsorbent for Removal of Itaconic Acid from Aqueous Solutions: Equilibrium and Kinetic Study. *Journal of The Turkish Chemical Society A* **2021**, *8*, 103–116, doi:10.18596/jotcsa.
44. Ahmad, N.; Marlan, A.R.; Negara, S.P.J. Insight of Anionic Dyes Adsorption from Their Aqueous Solutions onto MgAl LDH/Lignin: Characterization and Isotherm Studies. *Indonesian Journal of Material Research* **2024**, *2*, 40–46, doi:10.26554/ijmr.20242233.
45. Saleh, T.A. Chapter 3 - Kinetic Models and Thermodynamics of Adsorption Processes: Classification. In *Interface Science and Technology*; Saleh, T.A., Ed.; Elsevier, 2022; Vol. 34, pp. 65–97 ISBN 1573-4285.
46. Chen, Z.; Deng, H.; Zhang, M.; Yang, Z.; Hu, D.; Wang, Y.; Yan, K. One-Step Facile Synthesis of Ickel-Chromium Layered Double Hydroxide Nanoflakes for High-Performance Supercapacitors. *Nanoscale Adv* **2020**, *2*, 2099–2105, doi:10.1039/d0na00178c.
47. Gamil, S.; Antuch, M.; Zedan, I.T.; El Rouby, W.M.A. 3D NiCr-Layered Double Hydroxide/Reduced Graphene Oxide Sand Rose-Like Structure as Bifunctional Electrocatalyst for Methanol Oxidation. *Colloids Surf A Physicochem Eng Asp* **2020**, *602*, 125076, doi:10.1016/j.colsurfa.2020.125067.
48. Jefri, Fithri, N.A.; Arsyad, F.S.; Mardiyanto; Hanifa, Y.; Lesbani, A. Boosting Photocatalytic Efficiency: LDH Modified with Gambier Leaf Extract for Tetracycline Degradation. *Next Materials* **2025**, *7*, 100633, doi:10.1016/J.NXMATE.2025.100633.
49. Xia, J.; Wang, D.; Liang, P.; Zhang, D.; Du, X.; Ni, D.; Yu, Z. Vibrational (FT-IR, Raman) Analysis of Tea Catechins Based on Both Theoretical Calculations and Experiments. *Biophys Chem* **2020**, *256*, 106282, doi:10.1016/J.BPC.2019.106282.
50. Manalu, R.N.; Zahara, Z.A.; Mohadi, R. Ni-Cr Layered Double Hydroxide/Microcrystalline Cellulose Composite as Adsorbents for Malachite Green Dye. *Indonesian Journal of Material Research* **2023**, *1*, 51–60, doi:10.26554/ijmr.2023128.
51. Kurnosenko, S.A.; Silyukov, O.I.; Rodionov, I.A.; Baeva, A.S.; Burov, A.A.; Kulagina, A. V.; Novikov, S.S.; Zvereva, I.A. Hydrothermally Synthesized ZnCr- and NiCr-Layered Double Hydroxides as Hydrogen Evolution Photocatalysts. *Molecules* **2024**, *29*, 2108, doi:10.3390/molecules29092108.
52. Feng, X.; Li, X.; Su, B. Photocatalytic Degradation Performance of Antibiotics by Peanut Shell Biochar Anchored NiCr-LDH Nanocomposites Fabricated by One-Pot Hydrothermal Protocol. *Colloids Surf A Physicochem Eng Asp* **2023**, *666*, 131337, doi:10.1016/J.COLSURFA.2023.131337.
53. Dragan, G.; Kutarov, V.; Schieferstein, E.; Iorgov, A. Adsorption Hysteresis in Open Slit-Like Micropores. *Molecules* **2021**, *26*, doi:10.3390/molecules26165074.
54. Badri, A.F.; Juleanti, N.; Mohadi, R.; Mardiyanto; Lesbani, A. The Efficiency of Mg-Al/Biochar for Methyl Orange and Methyl Red Removal. *Ecological Engineering and Environmental Technology* **2022**, *23*, 202–211, doi:10.12912/27197050/142971.
55. Lee, H.; Fiore, S.; Berruti, F. Adsorption of Methyl Orange and Methylene Blue on Activated Biocarbon Derived from Birchwood Pellets. *Biomass Bioenergy* **2024**, *191*, 107446, doi:10.1016/J.BIOMBIOE.2024.107446.

56. Hambisa, A.A.; Regasa, M.B.; Ejigu, H.G.; Senbeto, C.B. Adsorption Studies of Methyl Orange Dye Removal from Aqueous Solution Using Anchote Peel-Based Agricultural Waste Adsorbent. *Appl Water Sci* **2023**, *13*, doi:10.1007/s13201-022-01832-y.
57. Waheed, T.; Din, S. ud; Ming, L.; Ahmad, P.; Min, P.; Haq, S.; Khandaker, M.U.; Boukhris, I.; Faruque, M.R.I.; Rehman, F.U.; *et al.* Porous Hierarchical Ni/Mg/Al Layered Double Hydroxide for Adsorption of Methyl Orange from Aqueous Solution. *Nanomaterials* **2023**, *13*, doi:10.3390/nano13131943.
58. Alyasi, H.; Mackey, H.; McKay, G. Adsorption of Methyl Orange from Water Using Chitosan Bead-like Materials. *Molecules* **2023**, *28*, doi:10.3390/molecules28186561.
59. Lafi, R.; Abdellaoui, L.; Montasser, I.; Hafiane, A. Removal of Methyl Orange from Aqueous Solution onto Modified Extracted Cellulose from *Stipa Tenacissima* L. *Int J Environ Anal Chem* **2022**, *102*, 8124–8140, doi:10.1080/03067319.2020.1845663.
60. Abdel-Hady, E.E.; Hafez, S.H.M.; Mohamed, H.F.M.; Elsharkawy, M.R.M. Characterization and Application of LDH with Chitosan Composites Investigated by Positron Annihilation Lifetime Spectroscopy and Surface Texture for the Adsorption of Methyl Orange. *Sci Rep* **2024**, *14*, doi:10.1038/s41598-024-65889-2.
61. Zaghoul, A.; Ait Ichou, A.; Benhiti, R.; Abali, M.; Soudani, A.; Chiban, M.; Zerbet, M.; Sinan, F. Removal of Methyl Orange from Aqueous Solution Using Synthetic Clay Type MgAl-LDH: Characterization, Isotherm and Thermodynamic Studies. *Mediterranean Journal of Chemistry* **2019**, *9*, 155, doi:10.13171/mjc92190925728fs.
62. Zhang, Z.; Wang, G.; Li, W.; Zhang, L.; Chen, T.; Ding, L. Degradation of Methyl Orange through Hydroxyl Radical Generated by Optically Excited Biochar: Performance and Mechanism. *Colloids Surf A Physicochem Eng Asp* **2020**, *601*, 125034, doi:<https://doi.org/10.1016/j.colsurfa.2020.125034>.
63. Wu, L.; Liu, X.; Lv, G.; Zhu, R.; Tian, L.; Liu, M.; Li, Y.; Rao, W.; Liu, T.; Liao, L. Study on the Adsorption Properties of Methyl Orange by Natural One-Dimensional Nano-Mineral Materials with Different Structures. *Sci Rep* **2021**, *11*, doi:10.1038/s41598-021-90235-1.
64. Al-Rub, S.S.A.; Alyami, B.A.; Alqahtani, Y.S.; Alqarih, A.R.; Dunquwah, B.A.; Alyami, M.M.; Alghithan, S.K.; Alsalah, H.H.; Aburub, A.S. Comparative Adsorption of Methyl Orange Color from an Aqueous Solution Using Activated Carbon. *Indian Journal of Pharmaceutical Education and Research* **2024**, *58*, 679–684, doi:10.5530/ijper.58.2.76.
65. Amri, A.; Wibiyani, S.; Wijaya, A.; Ahmad, N.; Mohadi, R.; Lesbani, A. Efficient Adsorption of Methylene Blue Dye Using Ni/Al Layered Double Hydroxide-Graphene Oxide Composite. *Bulletin of Chemical Reaction Engineering and Catalysis* **2024**, *19*, 181–189, doi:10.9767/bcrec.20121.
66. Rahayu Palapa, N.; Taher, T.; Mohadi, R.; Paluta Utami, H.; Lesbani, A. The Ability of Composite Ni/Al-Carbon Based Material Toward Readsorption of Iron(II) in Aqueous Solution. *Science and Technology Indonesia* **2021**, *6*, 156–165, doi:11.26554/sti.2221.6.3.156-165.
67. Bai, B.; Wang, Q.; Sun, Y.; Zhou, R.; Chen, G.; Tang, Y. Synthesis of Porous MgAl-LDH on a Micelle Template and Its Application for Efficient Treatment of Oilfield Wastewater. *Molecules* **2023**, *28*, doi:10.3390/molecules28186638.
68. Yadav; Dasgupta, S. Effect of Time, PH, and Temperature on Kinetics for Adsorption of Methyl Orange Dye into the Modified Nitrate Intercalated MgAl LDH Adsorbent. *Inorg Chem Commun* **2022**, *137*, 109203, doi:10.1016/j.inoche.2022.109203.
69. Hansen, P.E.; Spanget-Larsen, J. NMR and IR Investigations of Strong Intramolecular Hydrogen Bonds. *Molecules* **2017**, *22*, doi:10.3390/molecules22040552.
70. He, H.; Huang, Y.; Yan, M.; Xie, Y.; Li, Y. Synergistic Effect of Electrostatic Adsorption and Ion Exchange for Efficient Removal of Nitrate. *Colloids Surf A Physicochem Eng Asp* **2020**, *584*, 123973, doi:<https://doi.org/10.1016/j.colsurfa.2019.123973>.

Publisher's Note & Disclaimer

The statements, opinions, and data presented in this publication are solely those of the individual author(s) and contributor(s) and do not necessarily reflect the views of the publisher and/or the editor(s). The publisher and/or the editor(s) disclaim any responsibility for the accuracy, completeness, or reliability of the content. Neither the publisher nor the editor(s) assume any legal liability for any errors, omissions, or consequences arising from the use of the information presented in this publication. Furthermore, the publisher and/or the editor(s) disclaim any liability for any injury, damage, or loss to persons or property that may result from the use of any ideas, methods, instructions, or products mentioned in the content. Readers are encouraged to independently verify any information before relying on it, and the publisher assumes no responsibility for any consequences arising from the use of materials contained in this publication.